Supplement of Biogeosciences, 18, 251–283, 2021
https://doi.org/10.5194/bg-18-251-2021-supplement

Biogeosciences
Open Access

Supplement of

Factors controlling the competition between *Phaeocystis* and diatoms in the Southern Ocean and implications for carbon export fluxes

Cara Nissen and Meike Vogt

Correspondence to: Cara Nissen (cara.nissen@usys.ethz.ch)

Supplementary material

The supporting information provides additional figures in section S1 with respect to the nutrient limitation of phytoplankton growth in ROMS-BEC (S1), the ecological niche analysis (S2-S3), the data coverage in a SO satellite derived chlorophyll product (S4), the model evaluation (S5-S8), the bloom timing (S9), the competition sensitivity simulations (S10), carbon cycling in the Ross Sea (S11), and the results when using a varying half-saturation constant of iron for *Phaeocystis* growth (S12). In section S2, results of the parameter sensitivity simulations are described (Table S1-S3, Fig. S13).

S1: Additional figures

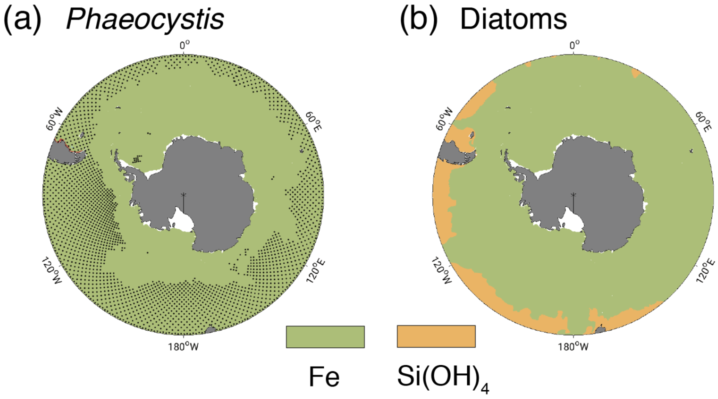

Figure S1: Annual mean most limiting nutrient at the surface south of 45° S for growth rates of a) *Phaeocystis* and b) diatoms in the *Baseline* simulation of ROMS-BEC. High-latitude phytoplankton growth in the model is most limited by either iron (green) or silicic acid (yellow, diatoms only). The stippling in panel a) denotes areas where peak monthly mean chlorophyll concentrations of Phaeocystis do not exceed 0.1 mg chl m^{-3}.

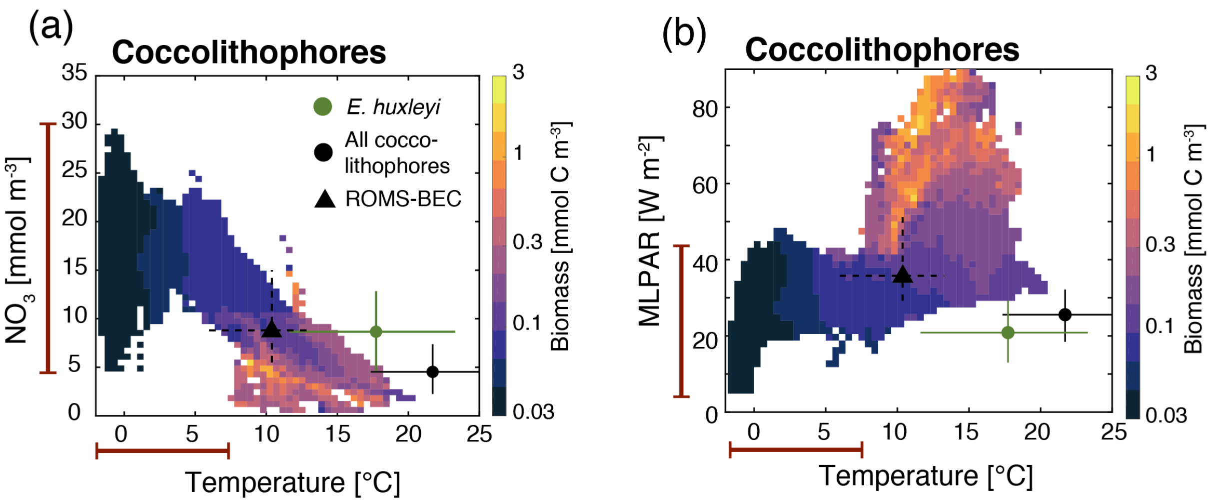

Figure S2: Simulated DJFM average top 50 m average coccolithophore carbon biomass concentrations (mmol C m^{-3}) south of 40° S as a function of the simulated temperature (° C) and a) nitrate concentrations (mmol N m^{-3}) and b) mixed layer PAR levels (W m^{-2}). Overlain are the observed ecological niche centers (median) and breadths (inter quartile ranges) for example taxa from Brun et al. (2015, circles and solid lines) and as simulated in ROMS-BEC (triangles and dashed lines; area and biomass weighted). The red bars on the axes indicate the simulated range of the respective environmental condition in ROMS-BEC between 60-90° S and averaged over DJFM and the top 50 m.

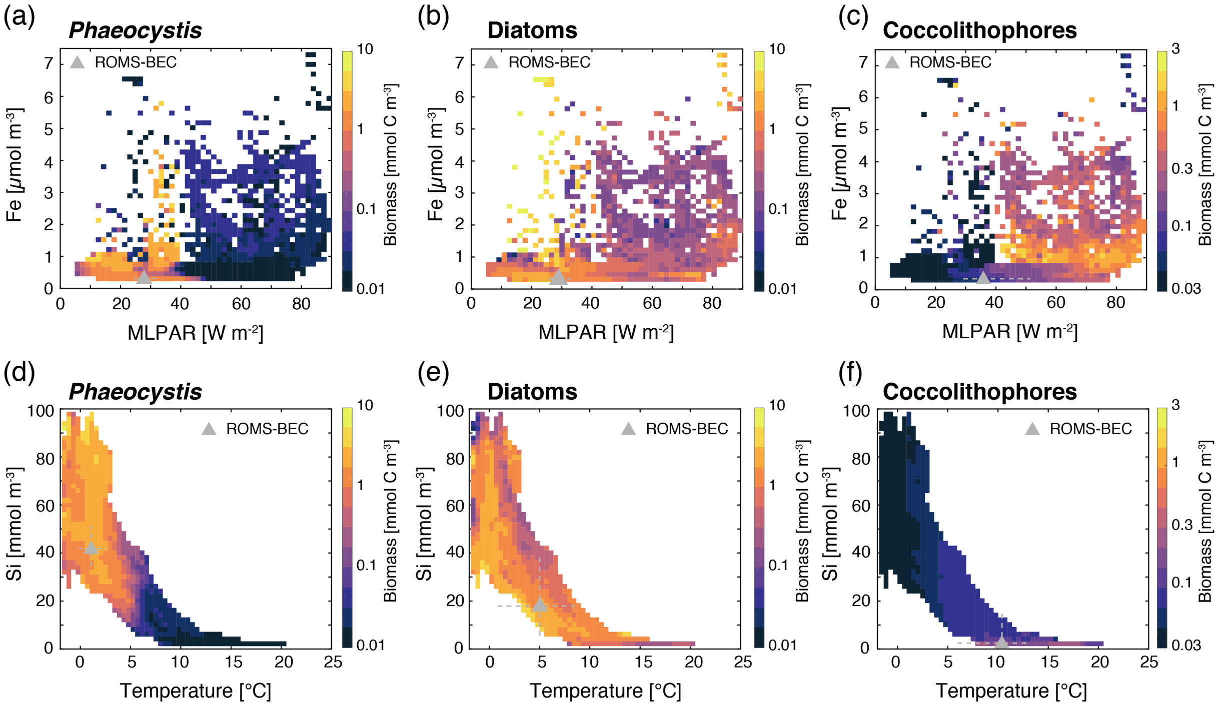

Figure S3: Simulated DJFM average top 50 m average a) *Phaeocystis*, b) diatom, and c) coccolithophore carbon biomass concentrations (mmol C m^{-3}) south of 40° S as a function of the simulated a)-c) dissolved iron concentrations (μmol Fe m^{-3}) and mixed layer PAR levels (W m^{-2}) and d)-f) temperature (° C) and dissolved silicic acid concentrations [mmol Si m^{-3}] in the 5-PFT *Baseline* simulation of ROMS-BEC. Overlain are the simulated area and biomass weighted ecological niche centers (median, triangle) and breadths (inter quartile ranges, dashed lines) for the three functional types.

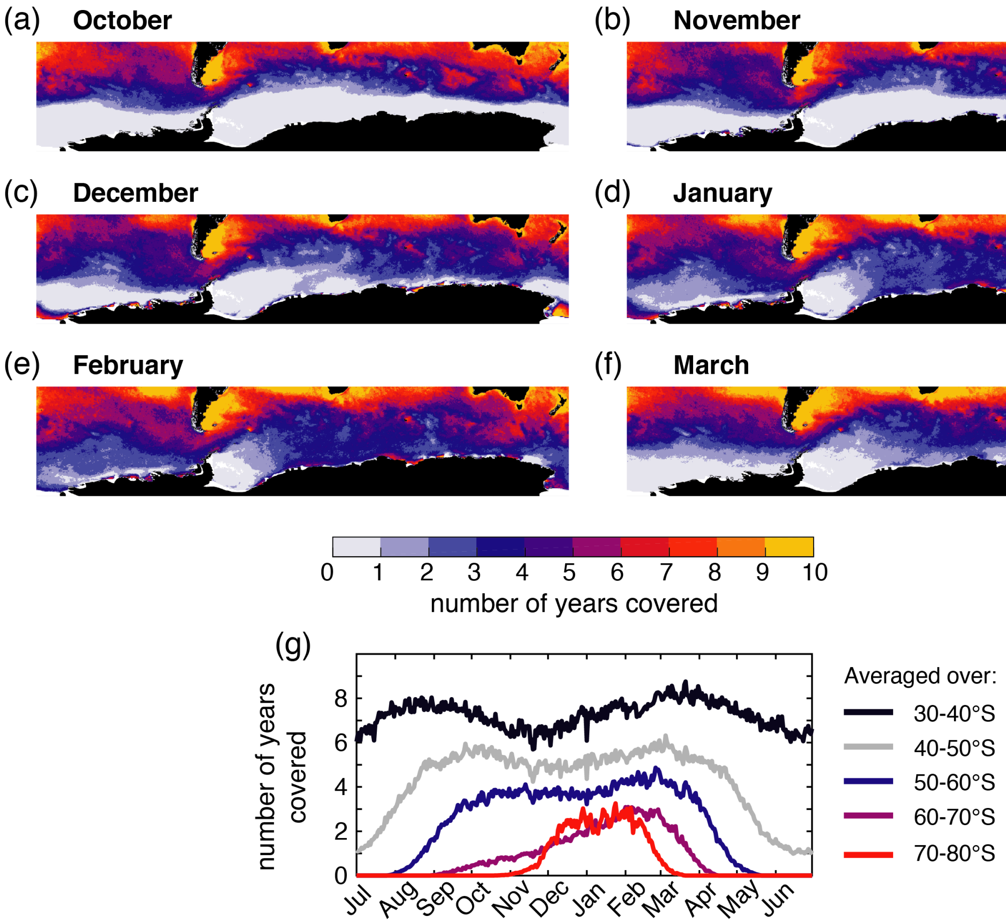

Figure S4: Assessment of the SO data coverage in the climatological (1998-2018, i.e. 21 years) daily Globcolor chlorophyll product (Fanton d'Andon et al., 2009; Maritorena et al., 2010): a)-f) Average number of years available for the calculation of the climatological chlorophyll concentration at each grid cell for each of the shown months (October-March), respectively. No minimum number of "days with data coverage" is required for a given month to be counted as "data available" (i.e. one day of data coverage in a month is enough for that month to be counted as "covered" in the respective year). g) Average number of years available for the calculation of the climatological chlorophyll concentration on each day for 10° latitudinal bands across the SO.

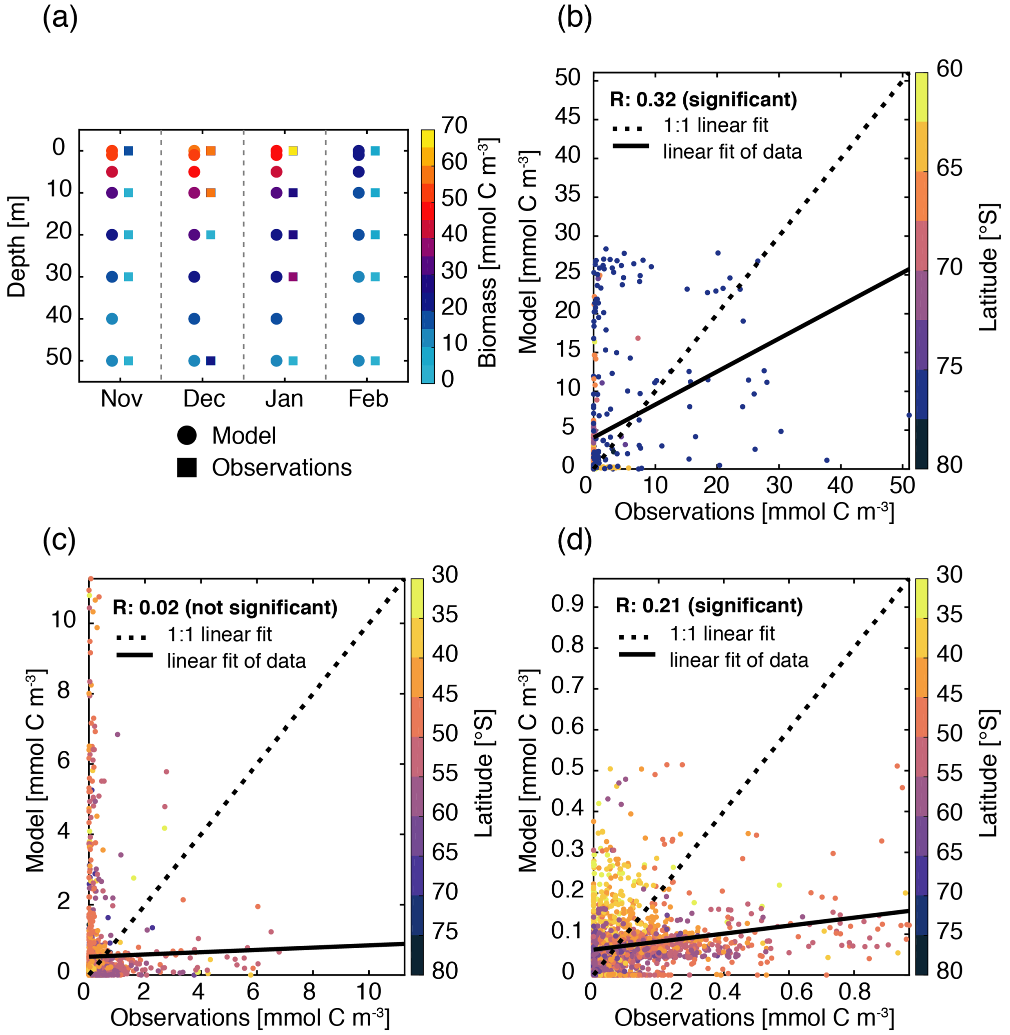

Figure S5: Validation of a) & b) *Phaeocystis*, c) diatom, and d) coccolithophore carbon biomass [mmol C m^{-3}]. Panel a) shows the maximum *Phaeocystis* carbon biomass concentrations [mmol C m^{-3}] in ROMS-BEC (circles) and in observations (squares, Vogt et al., 2012) for each month between November-February and in the the upper 50 meters of the water column. For panels b)-d), the model output is colocated with observations in space and time, and observational data from all months and from above 1000 m are considered here (Balch et al., 2016; Saavedra-Pellitero et al., 2014; O'Brien et al., 2013; Vogt et al., 2012; Leblanc et al., 2012; Tyrrell and Charalampopoulou, 2009; Gravalosa et al., 2008; Cubillos et al., 2007). For more details on the biomass evaluation, see Nissen et al. (2018). The dotted line shows the perfect linear 1:1 fit, whereas the solid line is the actual fit of the data (linear regression). Pearson correlation coefficients of these regressions are given in the top right, those for *Phaeocystis* and coccolithophores are statistically significant ($p<0.05$). Points are color-coded according to the sampling latitude.

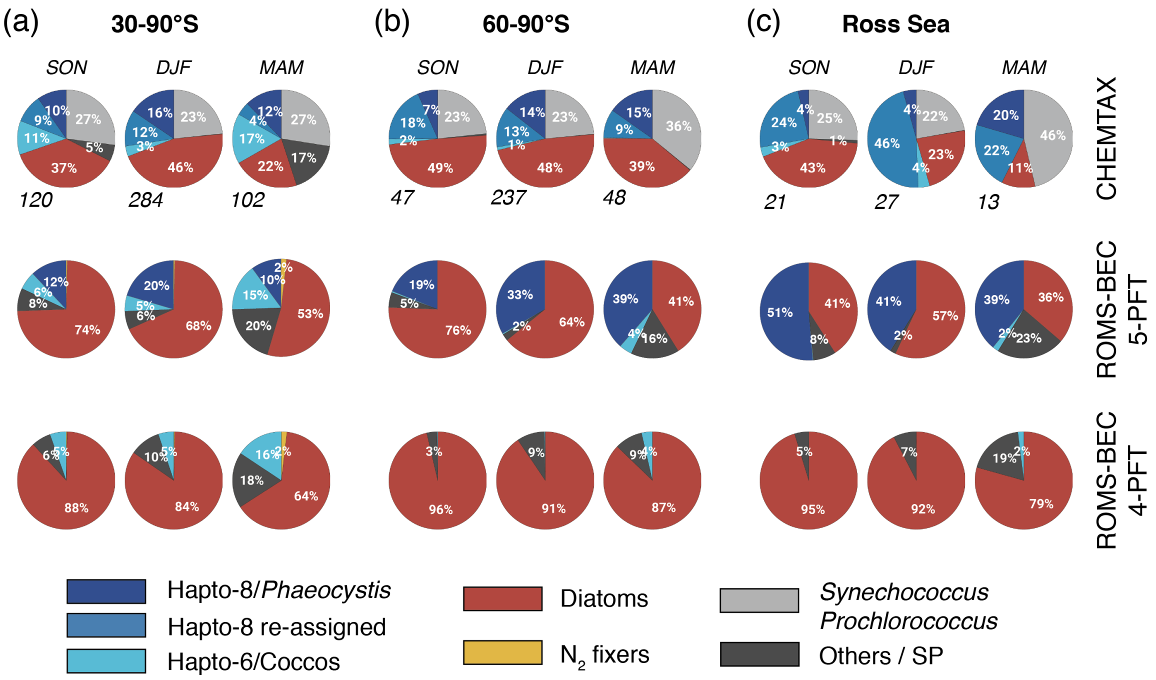

Figure S6: a)-c) Relative contribution of the five phytoplankton PFTs to total chlorophyll biomass [mg chl m^{-3}] for a) 30-90° S, b) 60-90° S, and c) the Ross Sea. The top pie charts denote the climatological mixed layer average community composition suggested by CHEMTAX analysis of HPLC pigments for spring, summer, and fall, respectively (the total number of available observations for a given region and season is given at the lower left side, Swan et al., 2016), and the lower pie charts denote the corresponding community structure in the top 50 m in ROMS-BEC in the 5-PFT setup (middle row, same as in Fig. 2 in the main text) and in the 4-PFT setup (lowest row, no *Phaeocystis*, Nissen et al., 2018), respectively. Note that the categories in the CHEMTAX analysis are not 100% equivalent to the model PFTs, and here, "Hapto-8 reassigned" corresponds to the contribution of Hapto-6 where the temperature is <2°C (see also section 2.3.1 in the main text).

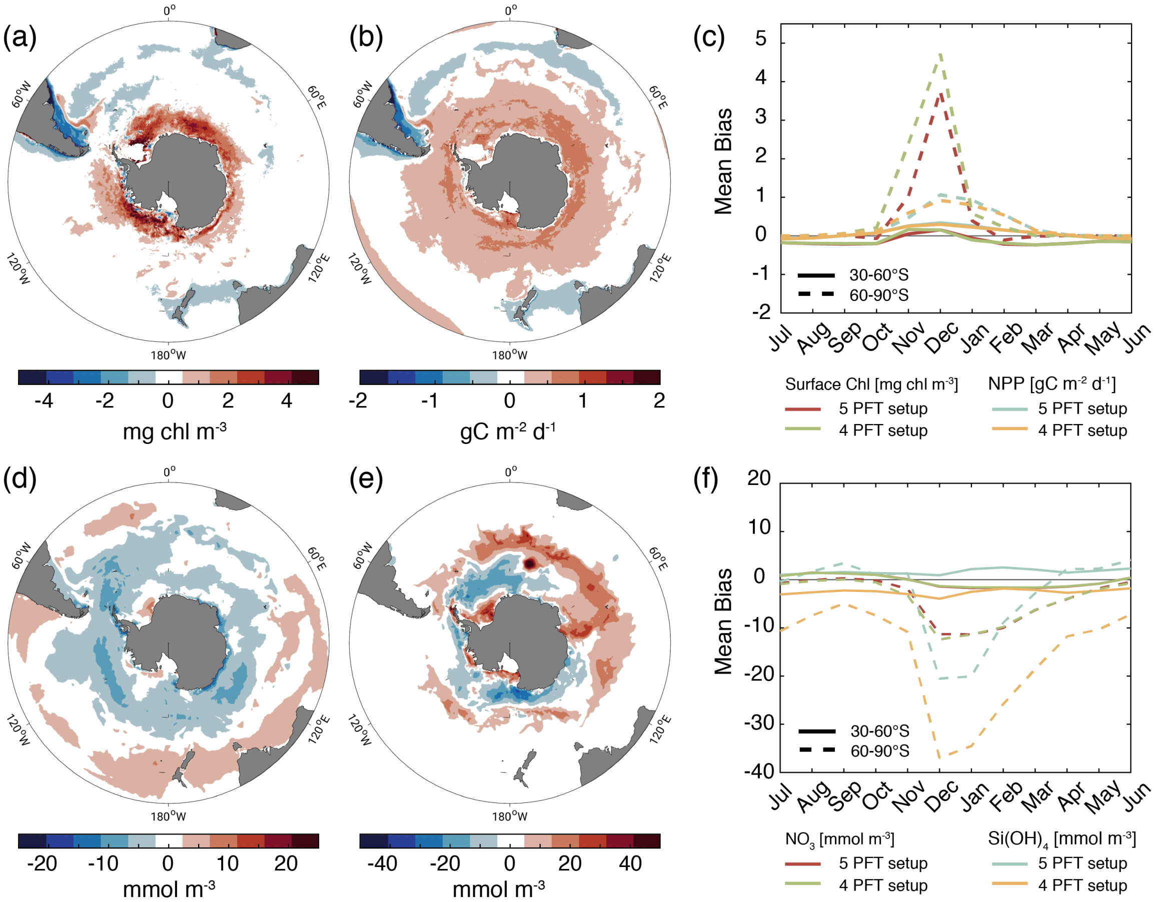

Figure S7: Annual mean bias (*Baseline* simulation minus observations) of a) total surface chlorophyll concentrations [g chl m^{-3}], b) total vertically integrated NPP [mg C m^{-2} d^{-1}], d) surface nitrate concentrations [mmol m^{-3}], and e) surface silicic acid concentrations [mmol m^{-3}]. The panels c) & f) denote the temporal evolution of the model bias of c) total surface chlorophyll concentration (red) and total NPP (blue), as well as f) surface nitrate concentrations (red), and silicic acid concentrations (blue) in the 5-PFT setup of ROMS-BEC between 30-60° S (solid) and 60-90° S (dashed), respectively. For comparison, the model bias obtained with the 4 PFT setup of ROMS-BEC is included in both panels in green (chlorophyll and nitrate) and yellow (NPP and silicic acid), respectively (see also supplement in Nissen et al., 2018).

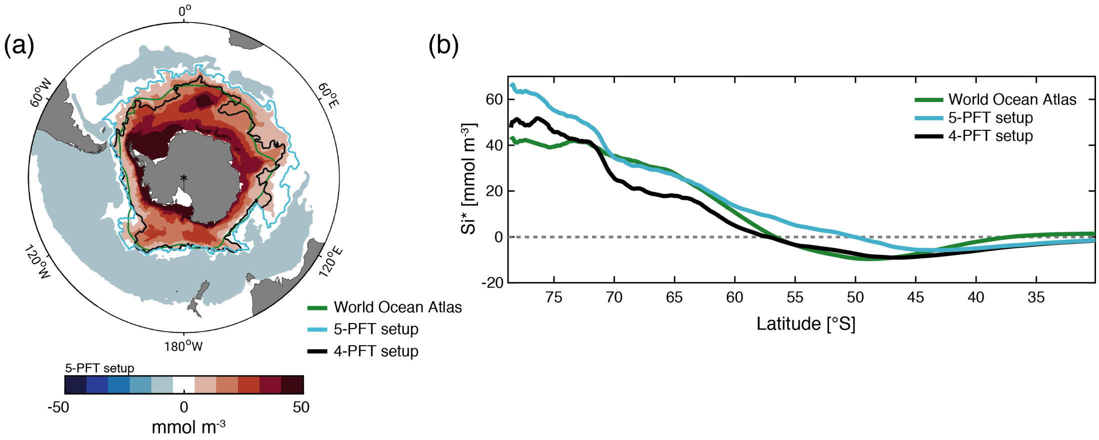

Figure S8: Annual mean top 100 m average a) Si* [mmol m^{-3}], which is defined as the difference in concentration between silicic acid and nitrate (Freeman et al., 2018), in the *Baseline* simulation of the 5-PFT setup of ROMS-BEC (colors). The contours denote the latitude of the silicate front, i.e. where Si*=0, in data from the World Ocean Atlas (green, Garcia et al., 2014) and in the *Baseline* simulation of the 5-PFT setup (light blue) and the 4-PFT setup (black, Nissen et al., 2018) of ROMS-BEC, respectively. b) zonal average Si* [mmol m^{-3}], colors are the same as the contours in panel a).

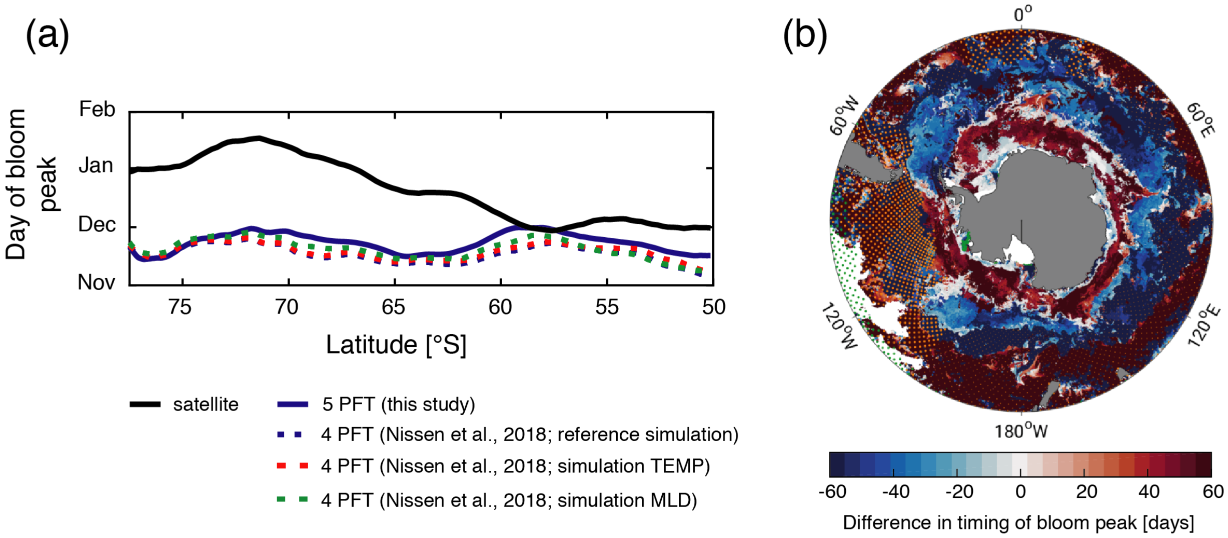

Figure S9: a) Same as Fig. 3 in the main text, Hovmoller plots south of 50° S of the day of maximum total chlorophyll concentrations in a satellite product (black line, Globcolor climatology from 1998-2018 based on the daily 25 km chlorophyll product, see Fanton d'Andon et al., 2009; Maritorena et al., 2010), the *Baseline* simulation of this study (solid blue line), the *Baseline* simulation of Nissen et al. (2018, dashed blue line; without *Phaeocystis*). Additionally, two sensitivity simulations in the 4 PFT setup from Nissen et al. (2018) are shown here to show the impact of biases in the simulated physical fields on phytoplankton phenology: The simulations TEMP (dashed red line) and MLD (dashed green line) correct for the simulated average temperature and MLD biases, respectively, within the biological subroutine of the model. b) Difference in day of bloom peak between *Phaeocystis* and diatoms, based on chlorophyll concentrations in the 5-PFT *Baseline* simulation. Stippling indicates locations where maximum chlorophyll concentrations never exceed 0.1 mg chl m^{-3} for *Phaeocystis* (orange) and diatoms (green), respectively. White areas correspond to areas where the peak total chlorophyll concentrations do not exceed 0.5 mg chl m^{-3}.

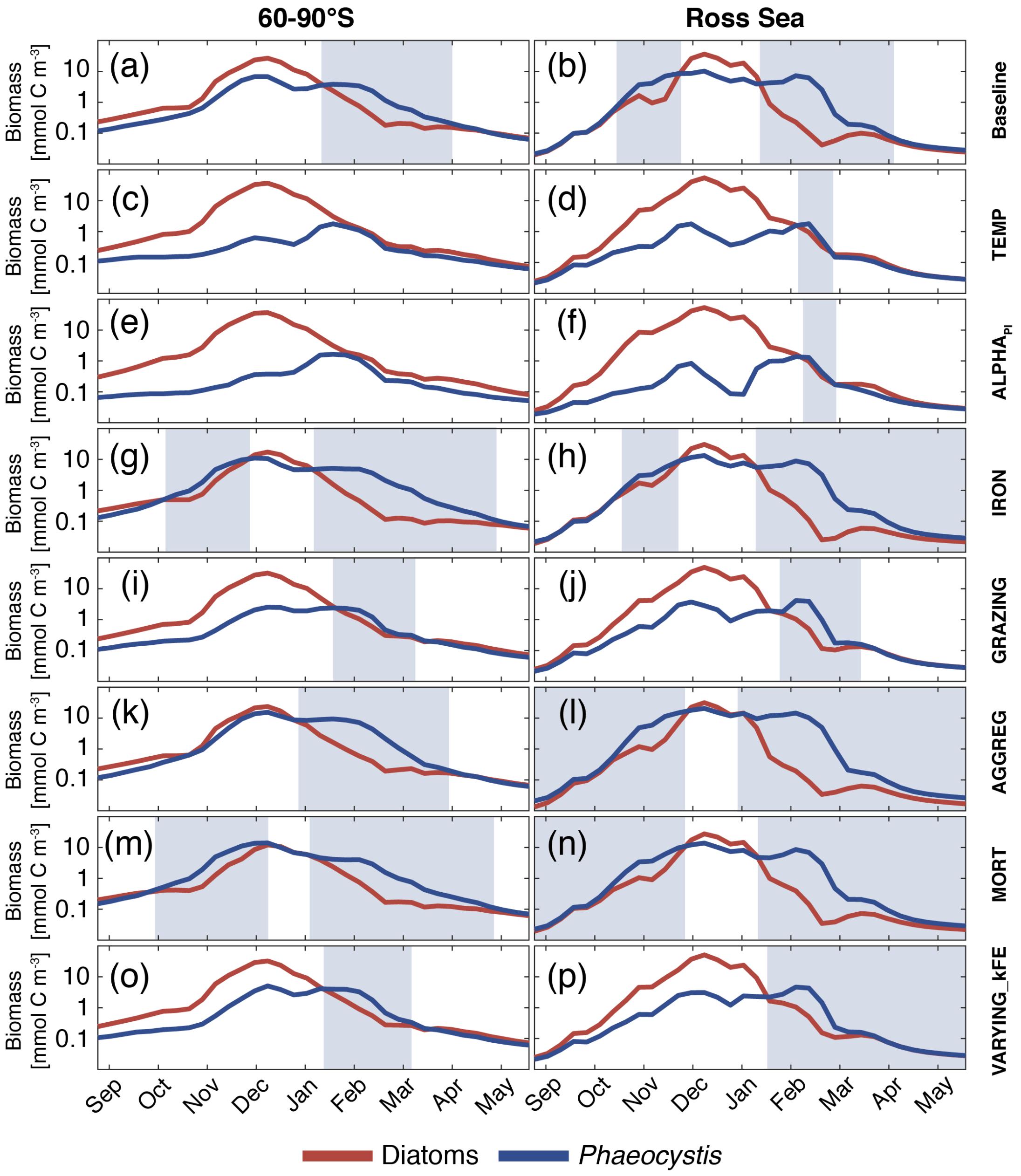

Figure S10: Diatom (red) and *Phaeocystis* (blue) surface carbon biomass concentrations [mmol C m^{-3}] in the different simulations performed in this study. See section 2.2. in the main text for details. The left panels are surface averages over 60-90° S and those on the right for the Ross Sea. Light blue area indicate times of the year when *Phaeocystis* biomass is larger than diatom biomass.

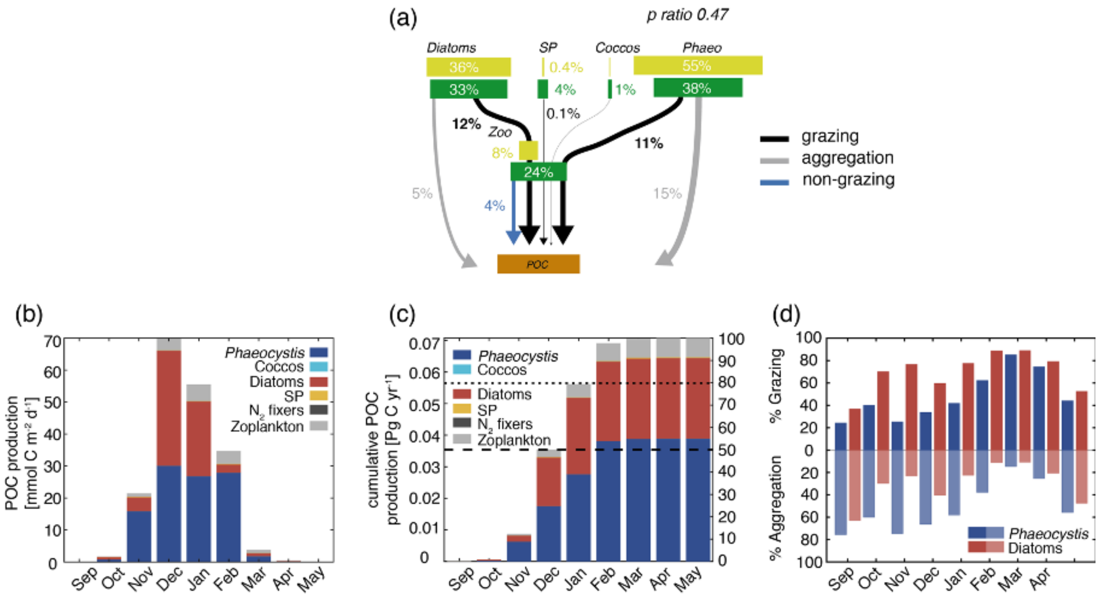

Figure S11: Carbon cycling in the Ross Sea: a) Pathways of particulate organic carbon (POC) formation in the *Baseline* simulation of ROMS-BEC averaged annually over the Ross Sea. The green and yellow boxes show the relative contribution (%) of *Phaeocystis*, diatoms, coccolithophores, small phytoplankton (SP), and zooplankton (Zoo) to the combined phytoplankton and zooplankton biomass (green) and total POC production (yellow) in the top 100 m, respectively. The arrows denote the relative contribution of the different POC production pathways associated with each PFT (black = grazing by zooplankton, grey = aggregation, blue = non-grazing mortality), given as % of total NPP in the top 100 m. Numbers are printed if ≥0.1% and rounded to the nearest integer if >1%. The sum of all arrows gives the POC production efficiency, i.e., the fraction of NPP which is converted into sinking POC upon biomass loss (p ratio). Note that diazotrophs are not included in this figure due to their minor contribution to NPP in the model domain. b)-d) Simulated vertically integrated production of particulate organic carbon (POC) b) as a function of time [mmol C m^{-2} d^{-1}], c) cumulative over time (absolute production in Pg C yr^{-1} on the left axis and relative to annually integrated production on the right axis), and d) as a function of time via grazing and aggregation, respectively. The colors correspond to the different PFTs in ROMS-BEC, and the panels correspond to averages or integrals over the Ross Sea.

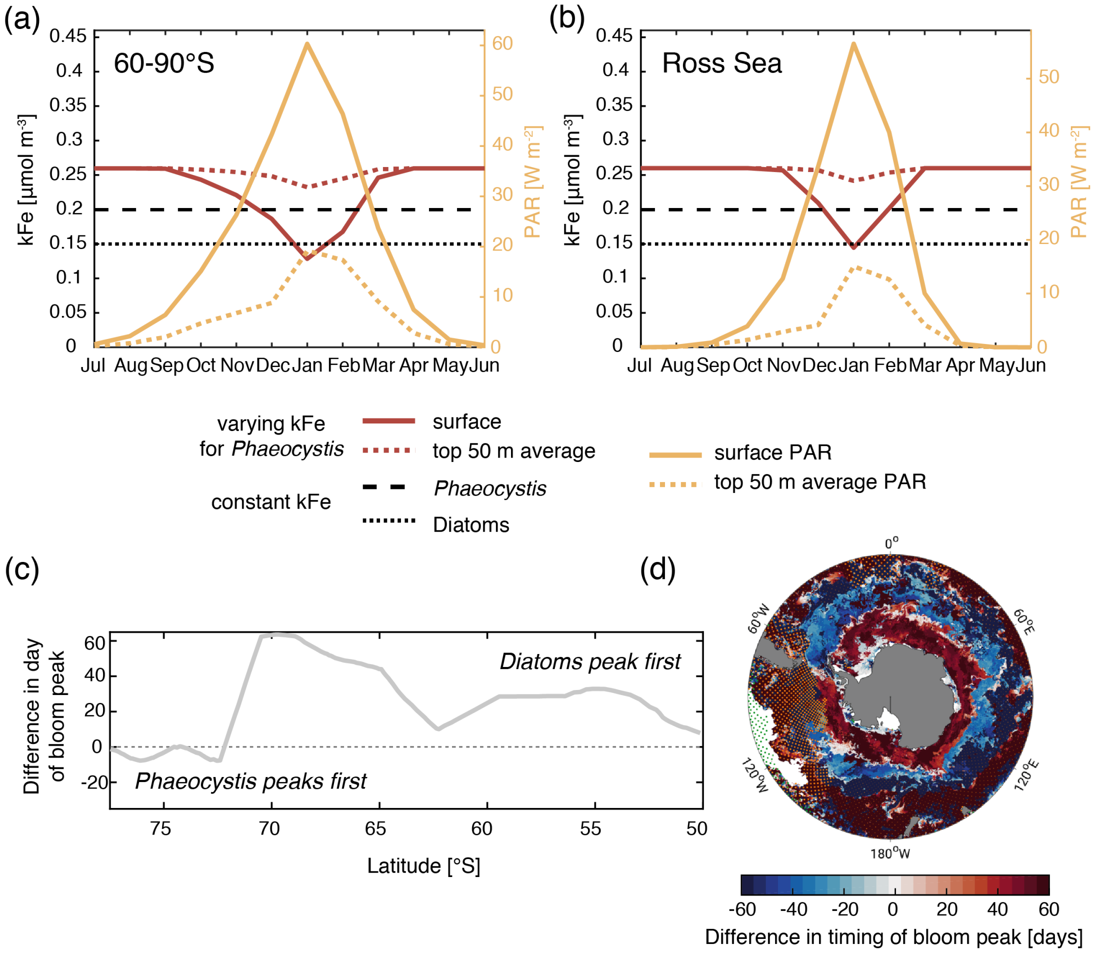

Figure S12: Results from the simulation VARYING_kFE (see section 2.2 in the main text): Varying half-saturation constant of iron of *Phaeocystis* (k_{Fe}, red, left y axis) and PAR (yellow, right y axis) as a function of time (x axis) for the surface (solid) and averaged over the top 50 m (dashed) for a) between 60-90° S and b) in the Ross Sea. Black lines indicate the constant k_{Fe} of *Phaeocystis* (dashed) and diatoms (dotted) used in the *Baseline* simulation of this study. c) Difference in days in the timing of the bloom peak of diatoms and *Phaeocystis* for each latitude, with negative values denoting a succession from *Phaeocystis* to diatoms throughout the season. d) Difference in day of bloom peak between *Phaeocystis* and diatoms. Stippling indicates locations where maximum chlorophyll concentrations never exceed 0.1 mg chl m^{-3} for *Phaeocystis* (orange) and diatoms (green), respectively. White areas correspond to areas where the peak total chlorophyll concentrations do not exceed 0.5 mg chl m^{-3}.

S2: Parameter sensitivity experiments

Table S1: Overview of parameter sensitivity simulations, varying the respective parameter by ±50%. PA=*Phaeocystis*, D=diatoms. See also Table 1 & Table 2 in the main text.

Run Name	**Description**	
Topt150	Increase $T_{\mathrm{opt}}^{\mathrm{PA}}$ by 50%	Param_Topt
Topt50	Decrease$T_{\mathrm{opt}}^{\mathrm{PA}}$ by 50%	
kFe150	Increase $k_{\mathrm{Fe}}^{\mathrm{PA}}$ by 50%	Param_kFe
kFe50	Decrease $k_{\mathrm{Fe}}^{\mathrm{PA}}$ by 50%	
alphaPI150	Increase $\alpha_{\mathrm{PI}}^{\mathrm{PA}}$ by 50%	Param_alphaPI
alphaPI50	Decrease $\alpha_{\mathrm{PI}}^{\mathrm{PA}}$ by 50%	
mortality150	Increase $\gamma_{\mathrm{m,0}}^{\mathrm{PA}}$ by 50%	Param_mortality
mortality50	Decrease $\gamma_{\mathrm{m,0}}^{\mathrm{PA}}$ by 50%	
aggregation150	Increase $\gamma_{\mathrm{a,0}}^{\mathrm{PA}}$ by 50%	Param_aggregation
aggregation50	Decrease $\gamma_{\mathrm{a,0}}^{\mathrm{PA}}$ by 50%	
grazing150	Increase $\gamma_{\mathrm{g,max}}^{\mathrm{PA}}$ by 50%	Param_grazing
grazing50	Decrease $\gamma_{\mathrm{g,max}}^{\mathrm{PA}}$ by 50%	
thetaNmax50	Increase $\theta_{\mathrm{chl:N,\,max}}^{\mathrm{PA}}$ by 50%	Param_thetaNmax
thetaNmax50	Decrease $\theta_{\mathrm{chl:N,\,max}}^{\mathrm{PA}}$ by 50%	

In order to more systematically quantify the sensitivity of simulated distributions of *Phaeocystis* and diatoms and integrated estimates of NPP and POC export in ROMS-BEC to *Phaeocystis* model parameter choices, we have performed a set of model parameter sensitivity experiments. To that aim, we have systematically increased/decreased all key *Phaeocystis* parameters by 50%, allowing for an objective ranking of model sensitivities. We varied the following seven parameters of *Phaeocystis*, resulting in a total of 14 simulations: the temperature optimum, the half-saturation constant of iron, α_{PI}, the maximum chl:N ratio $\theta_{\mathrm{chl:N,\,max}}$, the linear mortality rate, the quadratic mortality rate (aggregation), and the maximum grazing rate of zooplankton on *Phaeocystis* (see Table S1).

We then quantify the sensitivity S of any target variable A (here A being one of the following targets: total phytoplankton, *Phaeocystis*, and diatom chlorophyll concentrations, total NPP, and POC export across 100 m) to changes in the parameter X as follows, allowing for a ranking of the seven sets of simulations by the magnitude of the sensitivity (see Table S1):

$$S_{\mathrm{X}}^{A} = 100 \cdot \frac{A_{\mathrm{X150}} - A_{\mathrm{X50}}}{A_{\mathrm{X}\mathit{Baseline}}} \tag{1}$$

As expected (see also Nissen et al., 2018), we find that both total chlorophyll concentrations and chlorophyll levels of *Phaeocystis* and diatoms are highly sensitive to parameters describing the growth and loss of *Phaeocystis* biomass, with increases of up to 700% (grazing50) and declines of up to >90% (Topt50, thetaNmax50) in *Phaeocystis* biomass between 60-90° S for a 50% change in the associated parameters (see Fig. S13). In general, any decline/increase in *Phaeocystis* chlorophyll biomass is associated with an increase/decline in diatom chlorophyll biomass, pointing to the direct competition for resources of these two phytoplankton types at high SO latitudes. Yet, the biomass compensation is not always complete due to non-linearities in the model system (e.g. food web feedbacks), resulting in changes of up to 70% (grazing150) in total chlorophyll levels upon changes in *Phaeocystis* parameters. The ranking of model sensitivities between 60-90° S reveals the highest sensitivity of *Phaeocystis* and diatom chlorophyll concentrations to the maximum grazing rate $\gamma_{\mathrm{g,max}}^{\mathrm{PA}}$, the maximum chl:N ratio $\theta_{\mathrm{chl:N,\,max}}^{\mathrm{PA}}$, the initial slope of the photosynthesis-irradiance curve ($\alpha_{\mathrm{PI}}^{\mathrm{PA}}$), and the temperature optimum T_{opt} of *Phaeocystis* growth (Param_grazing, Param_thetaNmax, Param_alphaPI, Param_Topt

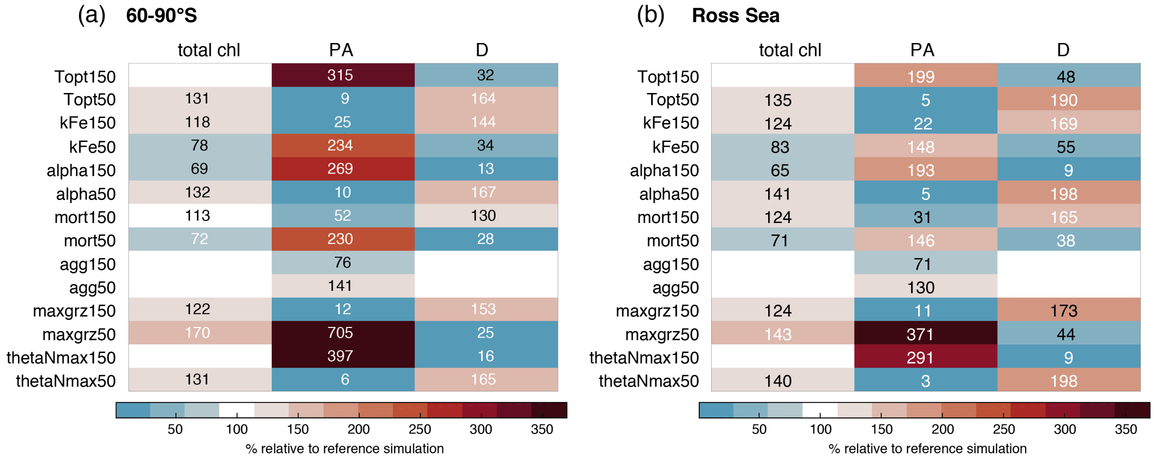

(a) 60-90°S

	total chl	PA	D
Topt150		315	32
Topt50	131	9	164
kFe150	118	25	144
kFe50	78	234	34
alpha150	69	269	13
alpha50	132	10	167
mort150	113	52	130
mort50	72	230	28
agg150		76	
agg50		141	
maxgrz150	122	12	153
maxgrz50	170	705	25
thetaNmax150		397	16
thetaNmax50	131	6	165

(b) Ross Sea

	total chl	PA	D
Topt150		199	48
Topt50	135	5	190
kFe150	124	22	169
kFe50	83	148	55
alpha150	65	193	9
alpha50	141	5	198
mort150	124	31	165
mort50	71	146	38
agg150		71	
agg50		130	
maxgrz150	124	11	173
maxgrz50	143	371	44
thetaNmax150		291	9
thetaNmax50	140	3	198

Figure S13: Annual mean surface chlorophyll concentrations of all phytoplankton (*total Chl*), *Phaeocystis* (*PA*), and diatoms (*D*) in the parameter sensitivity simulations (see Table S1) relative to the *Baseline* simulation. The model output is averaged over a) 60-90° S and b) the Ross Sea.

in Table S1 & S2). In comparison, the opposed changes in *Phaeocystis* and diatom chlorophyll levels (see Fig. S13) result in lower sensitivities of total chlorophyll levels to changes in *Phaeocystis* parameters in general and a lower ranking of the temperature optimum and thetaNmax experiments in particular (Param_Topt and Param_thetaNmax in Table S2).

In comparison to the ranking of model experiments for total chlorophyll, the model sensitivities for NPP and POC export across 100 m are similar in magnitude both between 60-90° S and in the Ross Sea (20-90%, compare Table S2 & Table S3). Additionally, the ranking of model experiments for NPP and POC export reveals only small differences to the ranking of model sensitivities for total chlorophyll: While the experiments Param_alphaPI and Param_grazing consistently rank amongst the top two most sensitive experiments for NPP and POC export and between 60-90° S for total chlorophyll concentrations, the experiments Param_mortality/Param_Topt are less/more important for NPP and POC than for total chlorophyll levels in ROMS-BEC (compare Table S2 & S3). In summary, this demonstrates the large model sensitivity of bulk biogeochemical quantities to parameter choices describing the temperature and light dependence of *Phaeocystis* growth and zooplankton grazing.

Table S2: Ranking of the parameter sensitivity experiments by the absolute sensitivity of annual mean total surface chlorophyll ($|S_{\mathrm{X}}^{\mathrm{Chl}}|$), *Phaeocystis* chlorophyll ($|S_{\mathrm{X}}^{\mathrm{Chl^{PA}}}|$), and diatom chlorophyll ($|S_{\mathrm{X}}^{\mathrm{Chl^{D}}}|$) to a ±50% change in the model parameter X relative to the *Baseline* setup of ROMS-BEC between 60-90°S and in the Ross Sea, respectively. The sensitivity S (%) is quantified using Eq. 1. See Table S1 for details on the experimental setup and Fig. S13 for details on the resulting chlorophyll fields in ROMS-BEC in each experiment. Note that the simulated changes in carbon biomass fields are qualitatively similar to those of chlorophyll (not shown) and that the ranking shown here is therefore insensitive to the choice of chlorophyll in the analysis.

	Ranking ($|\mathbf{S}_{\mathrm{X}}^{\mathrm{Chl}}|$ in %)	**Ranking ($|\mathbf{S}_{\mathrm{X}}^{\mathrm{Chl^{PA}}}|$ in %)**	**Ranking ($|\mathbf{S}_{\mathrm{X}}^{\mathrm{Chl^{D}}}|$ in %)**
60-90°S			
	1. Param_alphaPI (63.6)	1. Param_grazing (693.1)	1. Param_alphaPI (153.4)
	2. Param_grazing (48.3)	2. Param_thetaNmax (390.9)	2. Param_thetaNmax (149.6)
	3. Param_mortality (40.6)	3. Param_Topt (306.8)	3. Param_Topt (132.7)
	4. Param_kFe (39.8)	4. Param_alphaPI (259.4)	4. Param_grazing (128.3)
	5. Param_Topt (37.5)	5. Param_kFe (209.1)	5. Param_kFe (109.6)
	6. Param_thetaNmax (33.0)	6. Param_mortality (178.0)	6. Param_mortality (101.8)
	7. Param_aggregation (6.4)	7. Param_aggregation (65.1)	7. Param_aggregation (10.2)
Ross Sea			
	1. Param_alphaPI (76.3)	1. Param_grazing (360.3)	1. Param_thetaNmax (189.1)
	2. Param_mortality (53.3)	2. Param_thetaNmax (288.9)	2. Param_alphaPI (189.1)
	3. Param_thetaNmax (46.4)	3. Param_Topt (194.2)	3. Param_Topt (142.1)
	4. Param_Topt (41.6)	4. Param_alphaPI (188.3)	4. Param_grazing (129.8)
	5. Param_kFe (41.3)	5. Param_kFe (126.2)	5. Param_mortality (126.7)
	6. Param_grazing (19.2)	6. Param_mortality (114.8)	6. Param_kFe (114.3)
	7. Param_aggregation (12.3)	7. Param_aggregation (59.5)	7. Param_aggregation (9.0)

Table S3: Ranking of the parameter sensitivity experiments by the absolute sensitivity of annually integrated NPP ($|S_{\mathrm{X}}^{\mathrm{NPP}}|$) and POC export across 100 m ($|S_{\mathrm{X}}^{\mathrm{POC_{100m}}}|$) to a ±50% change in the model parameter X relative to the *Baseline* setup of ROMS-BEC between 60-90°S and in the Ross Sea, respectively. The sensitivity S (%) is quantified using Eq. 1. See Table S1 for the experimental setup.

	Ranking ($|\mathbf{S}_{\mathrm{X}}^{\mathrm{NPP}}|$ in %)	**Ranking ($|\mathbf{S}_{\mathrm{X}}^{\mathrm{POC_{100m}}}|$ in %)**
60-90°S		
	1. Param_grazing (68.4)	1. Param_grazing (86.4)
	2. Param_alphaPI (46.7)	2. Param_alphaPI (35.4)
	3. Param_Topt (43.6)	3. Param_Topt (26.7)
	4. Param_kFe (23.6)	4. Param_mortality (12.9)
	5. Param_thetaNmax (23.4)	5. Param_kFe (11.6)
	6. Param_mortality (11.6)	6. Param_thetaNmax (10.7)
	7. Param_aggregation (7.6)	7. Param_aggregation (1.4)
Ross Sea		
	1. Param_grazing (55.6)	1. Param_grazing (71.9)
	2. Param_alphaPI (48.5)	2. Param_alphaPI (39.0)
	3. Param_Topt (44.0)	3. Param_Topt (26.9)
	4. Param_thetaNmax (24.7)	4. Param_thetaNmax (11.9)
	5. Param_kFe (20.4)	5. Param_kFe (10.5)
	6. Param_aggregation (11.6)	6. Param_mortality (10.2)
	7. Param_mortality (8.3)	7. Param_aggregation (2.6)

References

Balch, W. M., Bates, N. R., Lam, P. J., Twining, B. S., Rosengard, S. Z., Bowler, B. C., Drapeau, D. T., Garley, R., Lubelczyk, L. C., Mitchell, C., and Rauschenberg, S.: Factors regulating the Great Calcite Belt in the Southern Ocean and its biogeochemical significance, Global Biogeochemical Cycles, 30, 1199–1214, https://doi.org/10.1002/2016GB005414, 2016.

Brun, P., Vogt, M., Payne, M. R., Gruber, N., O'Brien, C. J., Buitenhuis, E. T., Le Quéré, C., Leblanc, K., and Luo, Y.-W.: Ecological niches of open ocean phytoplankton taxa, Limnology and Oceanography, 60, 1020–1038, https://doi.org/10.1002/lno.10074, 2015.

Cubillos, J. C., Wright, S. W., Nash, G., de Salas, M. F., Griffiths, B., Tilbrook, B., Poisson, A., and Hallegraeff, G. M.: Calcification morphotypes of the coccolithophorid *Emiliania huxleyi* in the Southern Ocean: changes in 2001 to 2006 compared to historical data, Marine Ecology Progress Series, 348, 47–54, https://doi.org/10.3354/meps07058, 2007.

Fanton d'Andon, O., Mangin, A., Lavender, S., Antoine, D., Maritorena, S., Morel, A., Barrot, G., Demaria, J., and Pinnock, S.: GlobColour - the European Service for Ocean Colour, in: Proceedings of the 2009 IEEE International Geoscience & Remote Sensing Symposium, IEEE International Geoscience & Remote Sensing Symposium (IGARSS), ISBN: 9781424433957, 2009.

Freeman, N. M., Lovenduski, N. S., Munro, D. R., Krumhardt, K. M., Lindsay, K., Long, M. C., and Maclennan, M.: The variable and changing Southern Ocean silicate front: Insights from the CESM large ensemble, Global Biogeochemical Cycles, 32, 752–768, https://doi.org/10.1029/2017GB005816, 2018.

Garcia, H. E., Locarnini, R. A., Boyer, T. P., Antonov, J. I., Baranova, O. K., Zweng, M. M., Reagan, J. R., and Johnson, D. R.: World Ocean Atlas 2013, Volume 4 : Dissolved inorganic nutrients (phosphate, nitrate, silicate), NOAA Atlas NESDIS 76, 4, 25 pp, 2014.

Gravalosa, J. M., Flores, J.-A., Sierro, F. J., and Gersonde, R.: Sea surface distribution of coccolithophores in the eastern Pacific sector of the Southern Ocean (Bellingshausen and Amundsen Seas) during the late austral summer of 2001, Marine Micropaleontology, 69, 16–25, https://doi.org/10.1016/j.marmicro.2007.11.006, 2008.

Leblanc, K., Arístegui, J., Armand, L., Assmy, P., Beker, B., Bode, A., Breton, E., Cornet, V., Gibson, J., Gosselin, M.-P., Kopczynska, E., Marshall, H., Peloquin, J., Piontkovski, S., Poulton, A. J., Quéguiner, B., Schiebel, R., Shipe, R., Stefels, J., van Leeuwe, M. A., Varela, M., Widdicombe, C., and Yallop, M.: A global diatom database - abundance, biovolume and biomass in the world ocean, Earth System Science Data, 4, 149–165, https://doi.org/10.5194/essd-4-149-2012, 2012.

Maritorena, S., Fanton D'Andon, O., Mangin, A., and Siegel, D. A.: Merged satellite ocean color data products using a bio-optical model: Characteristics, benefits and issues, Remote Sensing of Environment, 114, 1791–1804, https://doi.org/10.1016/j.rse.2010.04.002, 2010.

Nissen, C., Vogt, M., Münnich, M., Gruber, N., and Haumann, F. A.: Factors controlling coccolithophore biogeography in the Southern Ocean, Biogeosciences, 15, 6997–7024, https://doi.org/10.5194/bg-15-6997-2018, 2018.

O'Brien, C. J., Peloquin, J. A., Vogt, M., Heinle, M., Gruber, N., Ajani, P., Andruleit, H., Arístegui, J., Beaufort, L., Estrada, M., Karentz, D., Kopczyńska, E., Lee, R., Poulton, A. J., Pritchard, T., and Widdicombe, C.: Global marine plankton functional type biomass distributions: coccolithophores, Earth System Science Data, 5, 259–276, https://doi.org/10.5194/essd-5-259-2013, 2013.

Saavedra-Pellitero, M., Baumann, K.-H., Flores, J.-A., and Gersonde, R.: Biogeographic distribution of living coccolithophores in the Pacific sector of the Southern Ocean, Marine Micropaleontology, 109, 1–20, https://doi.org/10.1016/j.marmicro.2014.03.003, 2014.

Swan, C. M., Vogt, M., Gruber, N., and Laufkötter, C.: A global seasonal surface ocean climatology of phytoplankton types based on CHEMTAX analysis of HPLC pigments, Deep-Sea Research Part I, 109, 137–156, https://doi.org/10.1016/j.dsr.2015.12.002, 2016.

Tyrrell, T. and Charalampopoulou, A.: Coccolithophore size, abundance and calcification across Drake Passage (Southern Ocean), 2009, https://doi.org/10.1594/PANGAEA.771715, 2009.

Vogt, M., O'Brien, C., Peloquin, J., Schoemann, V., Breton, E., Estrada, M., Gibson, J., Karentz, D., Van Leeuwe, M. A., Stefels, J., Widdicombe, C., and Peperzak, L.: Global marine plankton functional type biomass distributions: *Phaeocystis* spp., Earth System Science Data, 4, 107–120, https://doi.org/10.5194/essd-4-107-2012, 2012.